Supplement for "Stable Neo-Hookean Flesh Simulation"

BREANNAN SMITH, Pixar Animation Studios
FERNANDO DE GOES, Pixar Animation Studios
THEODORE KIM, Pixar Animation Studios

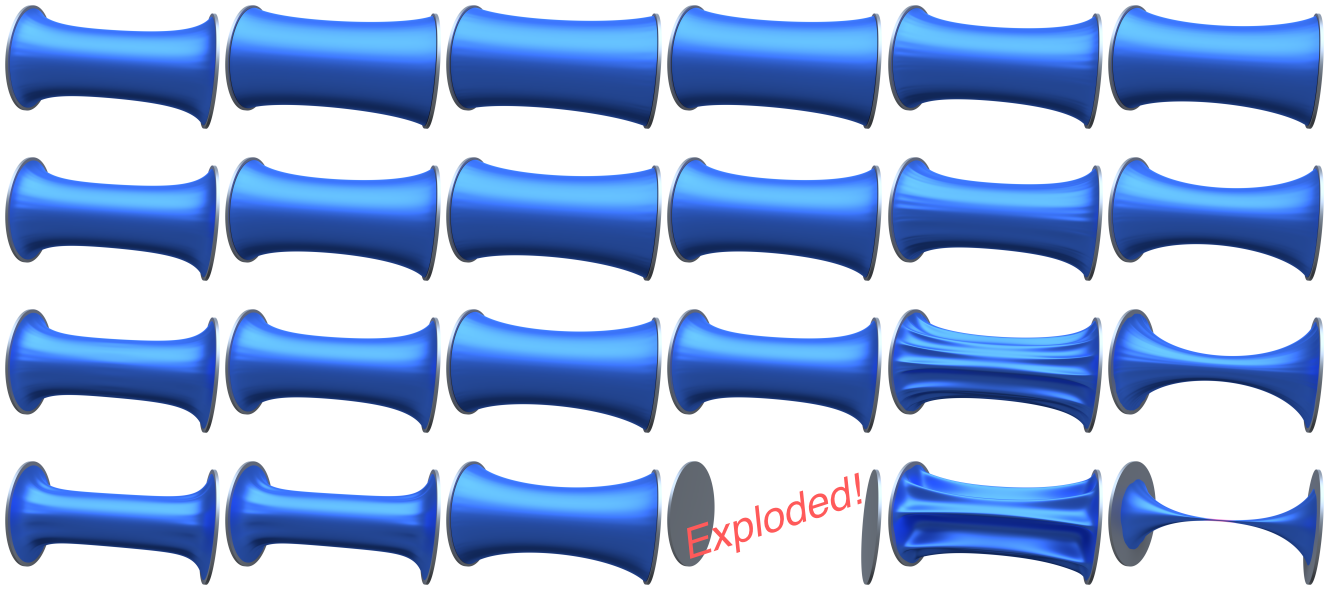

(a) Stable Neo-Hookean (b) Filtered Neo-Hookean [Teran et al. 2005] (c) Cubic Penalized StVK [Kikuuwe et al. 2009] (d) C_2 Neo-Hookean [Stomakhin et al. 2012] (e) Fixed Co-rotational [Stomakhin et al. 2012] (f) Co-rotational [Irving et al. 2004]

Fig. 1. Stretch test on a cylinder discretized with 306,406 hexahedra. The rows correspond respectively to $\nu = 0.2$, $\nu = 0.3$, $\nu = 0.4$ and $\nu = 0.49$. For the C_2 Neo-Hookean model at $\nu = 0.49$, we were unable to locate settings that completed the stretch test.

1 MODEL PERFORMANCE FOR MULTIPLE ν

In Fig. 1, we show the results of running the stretch test for a variety of Poisson's ratios ν across a variety of elasticity models:

- Our new energy.
- Neo-Hookean energy, filtered with Teran et al. [2005].
- St. Venant-Kirchhoff with a compression-resisting cubic penalty [Kikuuwe et al. 2009].
- The C_2 continuous extension of Neo-Hookean energy from Stomakhin et al. [2012].
- The "fixed" co-rotational energy from Stomakhin et al. [2012].
- The co-rotational energy from Irving et al. [2004].

The behavior of the three Neo-Hookean energies is very similar, although the slightly superior volume preservation of our model starts to be seen in the $\nu = 0.3$ row.

The "fixed" co-rotational model preserves volume, but unnatural crinkling artifacts start to appear even at small Poisson's ratios, e.g. $\nu = 0.2$. The original co-rotational model yields good results at $\nu = 0.2$, but quickly begins to lose volume at $\nu = 0.3$, and starts to severely invert at $\nu = 0.4$.

The StVK model with cubic compression resistance does not collapse like the co-rotational model, but instead gains significant volume (83%) under extension. This is expected, as the volumetric term deactivates under extension. The compression resistance term was set to $\kappa = 8 \times 10^8$. This setting was selected by running a sweep of elbow flexion simulations over the range $\kappa \in [0, 1.4 \times 10^9]$ for $\nu = 0.49$ and retaining the setting that exhibited the best volume preservation. Thus, these results are likely to be close to the highest quality that the model is able to produce.

2 META-STABILITY UNDER DEGENERACY

We examine the behavior of our initial energy,

$$\Psi = \frac{\mu}{2}(I_C - 3) - \mu(J - 1) + \frac{\lambda}{2}(J - 1)^2 \tag{1}$$

under three degenerate configurations: compression to a plane, line, and point.

2.1 Plane Degeneracy

We characterize a plane degeneracy by parameterizing $\mathbf{F}$ according to a compression term δ,

$$\mathbf{F} = \begin{bmatrix} \delta & 0 & 0 \\ 0 & 1 & 0 \\ 0 & 0 & 1 \end{bmatrix}. \tag{2}$$

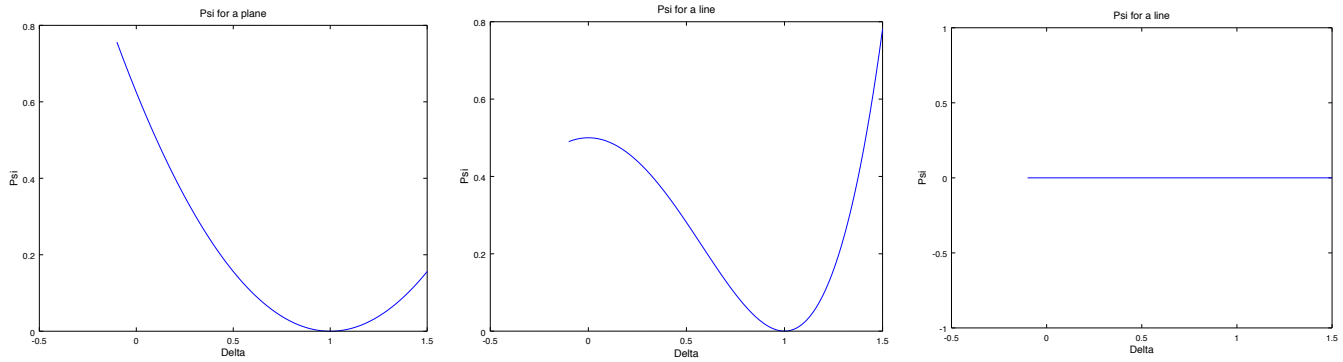

(a) Compression to a plane (b) Compression to a line (c) Compression to a line, $\nu = -\infty$

Fig. 2. Behavior of our initial energy, $\Psi = \frac{\mu}{2}(I_C - 3) - \mu(J-1) + \frac{\lambda}{2}(J-1)^2$, under various degenerate configurations.

The energy with respect to δ then becomes:

$$\Psi_{\text{plane}}(\delta) = \frac{\mu}{2}(\delta^2 - 1) - \mu(\delta - 1) + \frac{\lambda}{2}(\delta - 1)^2 \tag{3}$$

The energy is well-behaved under this degeneracy, as seen in Fig. 2(a). The energy has a minimum at $\delta = 1 \equiv \mathbf{F} = \mathbf{I}$, and increases elsewhere, including $\delta \leq 0$. It has this shape over the entire range $\nu \in [0, 0.5)$, where $\nu = 0.5$ is excluded because it corresponds to $\lambda = \infty$.

2.2 Line Degeneracy

We parameterize the line degeneracy as,

$$\mathbf{F} = \begin{bmatrix} \delta & 0 & 0 \\ 0 & \delta & 0 \\ 0 & 0 & 1 \end{bmatrix}, \tag{4}$$

and the energy with respect to δ then becomes:

$$\Psi_{\text{line}} = \frac{\mu}{2}(2\delta^2 - 2) - \mu(\delta^2 - 1) + \frac{\lambda}{2}(\delta^2 - \alpha)^2 \tag{5}$$

The energy is again well-behaved, as can be seen in Fig. 2(b). The energy again has a minimum at $\delta = 1 \equiv \mathbf{F} = \mathbf{I}$, but is now meta-stable at $\delta = 0$. In the absence of a singularity at $\delta = 0$, this is the correct behavior. If an unconstrained element has been crushed to a line, the rest shape that it should return to is no longer uniquely determined under rotation. Thus, it is meta-stable unless a tie-breaker such as momentum or an infinitesimal perturbation is introduced that selects an orientation.

The filtered forces from Teran et al. [2005] use the reflection convention as the tie-breaker. However, as observed by subsequent works [Civit-Flores and Susín 2014], the choice of reflection convention introduces new issues. When one singular value passes another in smallness, their orderings in Σ flip abruptly, which causes the direction of the restoring forces to flip, and introduces a force discontinuity.

Finally, when $\mu = 1$ and $\lambda = 0$, the energy resolves to zero, as seen in Fig. 2(c). Using the shifted Poisson's ratio for this model, $\nu = (\lambda - \mu)/(2\lambda)$, we see that this corresponds to $\nu = -\infty$. Thus, it is definitely well-behaved over the range of interest, $\nu \in [0, 0.5)$.

2.3 Point Degeneracy

Parameterizing by $\mathbf{F} = \delta\mathbf{I}$, we obtain $\Psi_{\text{point}} = \frac{\mu}{2}(3\delta^2 - 3) - \mu(\delta^3 - 1) + \frac{\lambda}{2}(\delta^3 - 1)^2$. For high Poisson's ratios, i.e. $\nu = 0.495 \equiv \mu = 1, \lambda = 100$, the energy resembles the line case, as seen in Fig. 3(a).

The same argument for meta-stability at $\delta = 0$ applies. If an element has been crushed to a point, the rest shape it should return to is ambiguous due to rotation. However, as the ratio is lowered, e.g. $\nu = 0.25 \equiv \mu = 1, \lambda = 2$, a spurious basin appears at $\delta = 0$ in Fig. 3(b). Then, as μ and λ approach parity, i.e. $\nu = 0 \equiv \mu = 1, \lambda = 1$, this minimum becomes energetically equivalent to the $\delta = 1$ minimum, as seen in Fig. 3(c). Finally, when $\lambda \to 0 \equiv \nu \to -\infty$, the $\delta = 0$ minimum becomes the preferred one and $\delta = 1$ becomes meta-stable in Fig. 3(d).

2.4 Adding a Regularized Origin Barrier

We have now identified two issues, both of which only appear under the point degeneracy:

- A stable basin appears at $\mathbf{F} = 0$ that grows as $\nu \to -\infty$.
- When $\nu = 0$, a basin appears at $\mathbf{F} = \mathbf{0}$ that is energetically identical to $\mathbf{F} = \mathbf{I}$.

We will introduce a new term that addresses both issues. Introducing a barrier term such as $\log I_C$ eliminates any basin of stability at $\mathbf{F} = 0$, but it also produces a singularity that we consider numerically unacceptable. Instead, we add a regularized barrier at the origin:

$$\Psi_{\text{b}} = \frac{\mu}{2}(I_C - 3) + \frac{\lambda}{2}(J - \alpha)^2 - \frac{\mu}{2}\log(I_C + \varepsilon) \tag{6}$$

We must now set ε to some positive value that eliminates both the $\mathbf{F} = 0$ basin and the log singularity.

We can derive an ε that accomplishes these goals. The Hessian of the original energy at $\mathbf{F} = 0$ is:

$$\mathbf{A}(\mathbf{F}) = \mu\mathbf{I} + \lambda\mathbf{g}\mathbf{g}^T + \lambda(J - \alpha)\mathbf{H} \tag{7}$$

$$\mathbf{A}(0) = \mu\mathbf{I} \tag{8}$$

The $\mu\mathbf{I}$ matrix is trivially positive definite, whereas we want to establish meta-stability by forcing $\mathbf{A}(0)$ to be zero or negative definite.

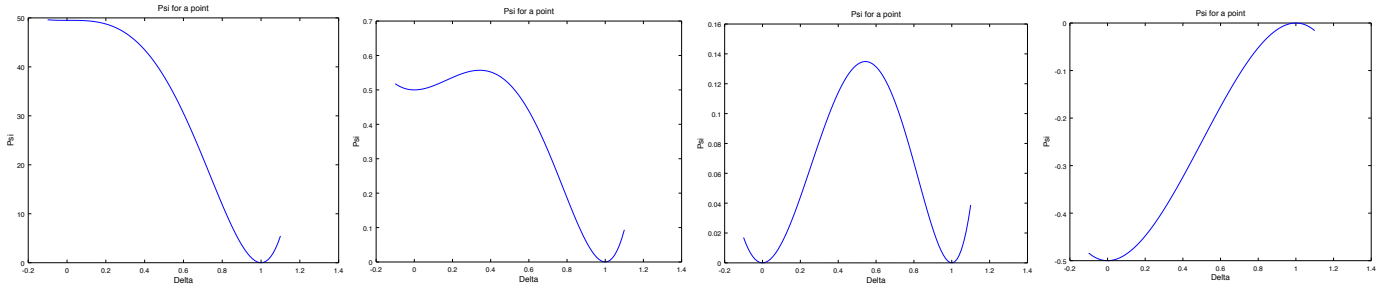

(a) $\nu = 0.495 \equiv \mu = 1, \lambda = 100$ (b) $\nu = 0.25 \equiv \mu = 1, \lambda = 2$ (c) $\nu = 0 \equiv \mu = 1, \lambda = 1$ (d) $\nu = -\infty \equiv \mu = 1, \lambda = 0$

Fig. 3. Behavior of the initial energy $\Psi = \frac{\mu}{2}(I_C - 3) - \mu(J-1) + \frac{\lambda}{2}(J-1)^2$ under uniform scaling for various Poisson's ratios ν. As ν decreases to $-\infty$, a spurious basin of stability appears about $\delta = 0$. At $\nu = 0$, the basin at $\delta = 0$ and $\delta = 1$ becomes energetically equivalent.

The Hessian of the energy at $\mathbf{F} = 0$ with the barrier term added is:

$$\mathbf{A}(\mathbf{F})_{\mathrm{b}} = \mu\left(1 - \frac{1}{I_C + \varepsilon}\right)\mathbf{I} + \lambda \mathbf{g}\mathbf{g}^T + \lambda(J-\alpha)\mathbf{H} + \frac{2\mu}{(I_C+\varepsilon)^2}\mathbf{f}\mathbf{f}^T \quad (9)$$

$$\mathbf{A}(0)_{\mathrm{b}} = \mu\left(1 - \frac{1}{\varepsilon}\right)\mathbf{I} \quad (10)$$

Setting $\varepsilon = 1$ will eliminate $\mathbf{F} = 0$ as a local minimum, and accomplishes the intended goal, as seen in Figure 4 The spurious basin

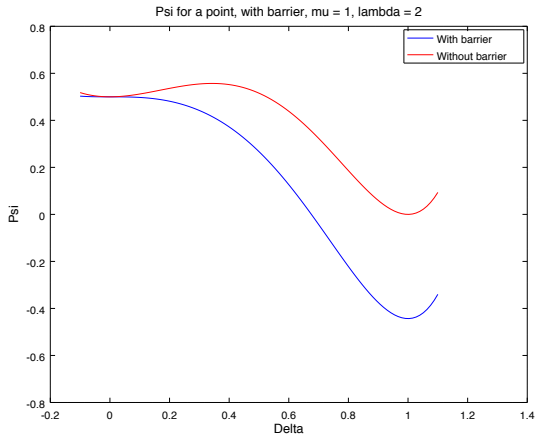

Fig. 4. Energy under uniform scaling both with (in blue) and without (in red) the origin barrier. In both plots, $\mu = 1$, $\lambda = 2$. With the origin barrier added, the basin at $\delta = 0$ is clearly eliminated. The red plot without the origin barrier is the same as Fig. 3(b), but scaled to accommodate the range of the other plot.

of stability at $\mathbf{F} = 0$ has now been eliminated for all $\nu \in [0, 0.5)$. For completeness, we now compute the ν at which $\mathbf{F} = \mathbf{I}$ becomes meta-stable. The point degeneracy, including the barrier, is:

$$\Psi_{\mathrm{b,point}} = \frac{\mu}{2}(3\delta^2 - 3) - \mu\left(\frac{3}{4}\delta^3 - 1\right) + \frac{\lambda}{2}(\delta^3 - 1)^2 - \frac{\mu}{2}\log\left(3\delta^2 + 1\right) \quad (11)$$

The meta-stable point first appears when λ turns $\Psi_{\mathrm{b,point}}(1)$ into an inflection point, i.e. when λ makes $\frac{\partial^2 \Psi_{\mathrm{b,point}}(1)}{\partial \delta^2} = 0$. For general ε, this occurs when:

$$\lambda = \left[\frac{1}{3} - \frac{1}{3+\varepsilon}\left(\frac{1}{3} + \frac{2}{3+\varepsilon}\right)\right]\mu \quad (12)$$

For $\varepsilon = 1$, this corresponds to $\lambda = \frac{\mu}{8}$. Using the Poisson's ratio formula $\nu = \frac{\lambda - 5/8\mu}{2(\lambda + 1/8\mu)}$, this means $\mathbf{F} = \mathbf{I}$ becomes meta-stable when $\nu = -1$. At this exact setting of ν, some oscillations appear around $\mathbf{F} = \mathbf{I}$ due to the presence of the inflection point, as seen in Fig. 5(a).

At $\lambda = 1/4, \mu = 1 \equiv \nu = -1/2$, these oscillations already begin to smooth out, as seen in Fig. 5(c). Finally, when $\lambda = \frac{5}{8}, \mu = 1 \equiv \nu = 0$, the oscillation has smoothed out completely, as seen in Fig. 5(d). Thus, adding the regularized origin barrier has guaranteed that our model is well-behaved under point, line, and plane degeneracies, over the range of $\nu \in [0, 0.5)$. It appears that the material will also give stable results in the auxetic regime as well, but there is no reason to expect that these results will be accurate.

2.5 The Final Energy

The final energy is:

$$\Psi_{\mathrm{b}} = \frac{\mu}{2}(I_C - 3) + \frac{\lambda}{2}(J-\alpha)^2 - \frac{\mu}{2}\log(I_C + 1) \quad (13)$$

The α that preserves rest-stability is $\alpha = 1 + \frac{\mu}{\lambda} - \frac{\mu}{4\lambda}$, so expanding α out of the quadratic yields:

$$\Psi = \frac{\mu}{2}(I_C - 3) - \mu\left(\frac{3J}{4} - 1\right) + \frac{\lambda}{2}(J-1)^2 - \frac{\mu}{2}\log(I_C + 1) \quad (14)$$

The PK1 becomes:

$$\mathbf{P} = \mu\mathbf{F} - \mu\frac{3}{4}\frac{\partial J}{\partial \mathbf{F}} + \lambda(J-1)\frac{\partial J}{\partial \mathbf{F}} - \frac{\mu}{I_C + 1}\mathbf{F} \quad (15)$$

$$= \mu\left(1 - \frac{1}{I_C+1}\right)\mathbf{F} + \left(\lambda(J-1) - \frac{3}{4}\mu\right)\frac{\partial J}{\partial \mathbf{F}}, \quad (16)$$

the Hessian is then,

$$\begin{aligned}\frac{\partial \mathbf{P}}{\partial \mathbf{F}_{ij}} =& \mu\frac{\partial \mathbf{F}}{\partial \mathbf{F}_{ij}} - \frac{3}{4}\mu\frac{\partial^2 J}{\partial \mathbf{F}\partial \mathbf{F}_{ij}} + \lambda\frac{\partial J}{\partial \mathbf{F}_{ij}}\frac{\partial J}{\partial \mathbf{F}} + \\ & \lambda(J-1)\frac{\partial^2 J}{\partial \mathbf{F}\partial \mathbf{F}_{ij}} - \frac{\mu}{I_C+1}\frac{\partial \mathbf{F}}{\partial \mathbf{F}_{ij}} + \frac{2\mu}{(I_C+1)^2}\mathbf{F}_{ij}\mathbf{F},\end{aligned} \quad (17)$$

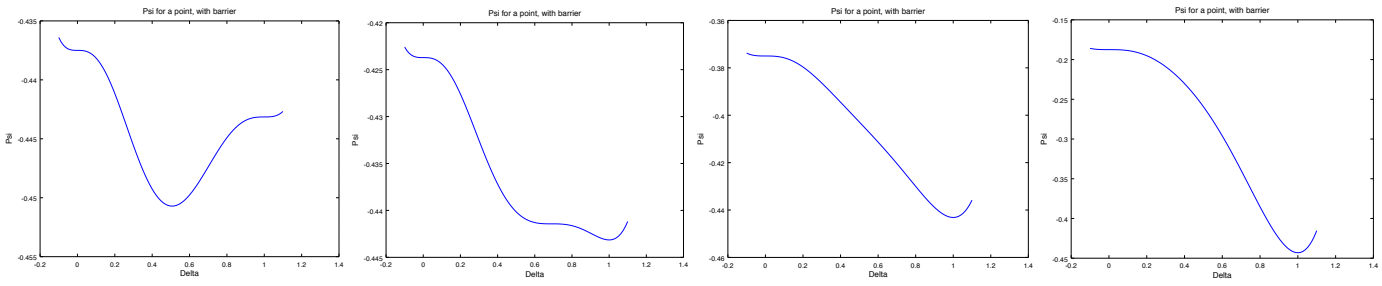

(a) $\nu = -1 \equiv \mu = 1, \lambda = 1/8$ (b) $\nu = -0.851 \equiv \mu = 1, \lambda = 0.1526$ (c) $\nu = -1/2 \equiv \mu = 1, \lambda = 1/4$ (d) $\nu = 0 \equiv \mu = 1, \lambda = 5/8$

Fig. 5. Behavior of the energy under uniform scaling with an origin barrier added, $\Psi_b = \frac{\mu}{2}(I_C - 3) + \frac{\lambda}{2}(J - \alpha)^2 - \frac{\mu}{2}\log(I_C + 1)$, as the Poisson's ratio increases from -1 to 0. The -0.851 threshold was found numerically to be the transition point where a spurious critical point disappears. By $\nu = -1/2$, the oscillation has smoothed out, and by $\nu = 0$, it has disappeared entirely.

which flattens to

$$\begin{aligned}\mathbf{A} =& \mu\left(1 - \frac{1}{I_C + 1}\right)\mathbf{I} + \left(\lambda(J-1) - \frac{3}{4}\mu\right)\mathbf{H} + \\ & \lambda\mathbf{g}\mathbf{g}^T + \frac{2\mu}{(I_C+1)^2}\mathbf{f}\mathbf{f}^T.\end{aligned} \tag{18}$$

The complete eigensystem for this energy is given in the main document.

3 ENERGY MINIMA FOR STABLE NEO-HOOKEAN ELASTICITY

We would like to determine the conditions under which our Stable Neo-Hookean energy contains spurious minima that do not correspond to pure rotations. We address this question in two stages. First, we show that minima can only appear during uniform scaling, i.e. when all the singular values σ_i are equal. Then, with the uniform scaling mode isolated, will locate Poisson's ratios under which the desirable minima appear.

3.1 Minima Only Appear Under Uniform Scaling

We denote the SVD of the deformation gradient $\mathbf{F}$ as:

$$\mathbf{F} = \mathbf{U}\Sigma\mathbf{V}^T \quad \text{and} \quad \Sigma = \begin{bmatrix} \sigma_0 & 0 & 0 \\ 0 & \sigma_1 & 0 \\ 0 & 0 & \sigma_2 \end{bmatrix}. \tag{19}$$

The PK1 in the principal stretch space spanned by Σ is then:

$$\mathbf{P}(\Sigma) = \mu\left(1 - \frac{1}{I_C+1}\right)\Sigma + \lambda\left(J - 1 - \frac{\mu}{\lambda} + \frac{\mu}{4\lambda}\right)\frac{\partial J}{\partial \mathbf{F}} \tag{20}$$

$$= \mu\left(1 - \frac{1}{I_C+1}\right)\begin{bmatrix} \sigma_0 & 0 & 0 \\ 0 & \sigma_1 & 0 \\ 0 & 0 & \sigma_2 \end{bmatrix} + \tag{21}$$

$$\left(\lambda(J-1) - \frac{3}{4}\mu\right)\begin{bmatrix} \sigma_1\sigma_2 & 0 & 0 \\ 0 & \sigma_0\sigma_2 & 0 \\ 0 & 0 & \sigma_0\sigma_1 \end{bmatrix} \tag{22}$$

We will now examine the conditions under which $\mathbf{P}(\Sigma) = \mathbf{0}$, which correspond to the critical points of Ψ up to rotation. This is equivalent to the general case, since $\mathbf{P}(\mathbf{0}) = \mathbf{U0V}^T = \mathbf{0}$. Showing the non-existence of critical points over a certain domain is a stronger test than locating the minima, since it also includes the maxima and saddle points. We can write $\mathbf{P}(\Sigma) = \mathbf{0}$ as a rational system:

$$\mu\left(1 - \frac{1}{I_C+1}\right)\sigma_0 + \left(\lambda(J-1) - \frac{3}{4}\mu\right)\sigma_1\sigma_2 = 0 \tag{23}$$

$$\mu\left(1 - \frac{1}{I_C+1}\right)\sigma_1 + \left(\lambda(J-1) - \frac{3}{4}\mu\right)\sigma_0\sigma_2 = 0 \tag{24}$$

$$\mu\left(1 - \frac{1}{I_C+1}\right)\sigma_2 + \left(\lambda(J-1) - \frac{3}{4}\mu\right)\sigma_0\sigma_1 = 0. \tag{25}$$

This can be made into a polynomial system by multiplying by (I_C+1) and further simplified by expanding $J = \sigma_0\sigma_1\sigma_2$. We also divide through by μ so that the system only contains one constant, $\beta = \frac{\lambda}{\mu}$.

$$\left(I_C + \beta(I_C+1)\sigma_1^2\sigma_2^2\right)\sigma_0 - \left(\beta + \frac{3}{4}\right)(I_C+1)\sigma_1\sigma_2 = 0 \tag{26}$$

$$\left(I_C + \beta(I_C+1)\sigma_0^2\sigma_2^2\right)\sigma_1 - \left(\beta + \frac{3}{4}\right)(I_C+1)\sigma_0\sigma_2 = 0 \tag{27}$$

$$\left(I_C + \beta(I_C+1)\sigma_0^2\sigma_1^2\right)\sigma_2 - \left(\beta + \frac{3}{4}\right)(I_C+1)\sigma_0\sigma_1 = 0. \tag{28}$$

We then exclude the uniform scaling mode from the solution space by imposing the following constraints:

$$\sigma_0 \neq \sigma_1 \qquad \sigma_0 \neq \sigma_2 \qquad \sigma_1 \neq \sigma_2. \tag{29}$$

We can then solve for all the real-valued critical points symbolically using Mathematica:

```
s0 =.
s1 =.
s2 =.
beta =.
IC = s0^2 + s1^2 + s2^2;
solution =
  Solve[{
  (IC + beta * s1^2 * s2^2 * (IC + 1)) * s0 -
  (3/4 + beta) * s1 * s2 * (IC + 1) == 0,
  (IC + beta * s0^2 * s2^2 * (IC + 1)) * s1 -
  (3/4 + beta) * s0 * s2 * (IC + 1) == 0,
  (IC + beta * s0^2 * s1^2 * (IC + 1)) * s2 -
  (3/4 + beta) * s0 * s1 * (IC + 1) == 0,
```

```
  s0 != s1, s0 != s2, s1 != s2}, {s0, s1, s2}, Reals]
```

After a lengthy computation (4.3 hours on a MacBook Pro), Mathematica returns the null set. No critical points exist over this domain. As a sanity check, we remove the uniform scaling constraints and set $\beta = 1$:

```
beta = 1
solution =
  Solve[{
  (IC + beta * s1^2 * s2^2 * (IC + 1)) * s0 -
  (3/4 + beta) * s1 * s2 * (IC + 1) == 0,
  (IC + beta * s0^2 * s2^2 * (IC + 1)) * s1 -
  (3/4 + beta) * s0 * s2 * (IC + 1) == 0,
  (IC + beta * s0^2 * s1^2 * (IC + 1)) * s2 -
  (3/4 + beta) * s0 * s1 * (IC + 1) == 0},
  {s0, s1, s2}, Reals]
```

Mathematica then returns the expected critical points, which all lie along the uniform scaling directions:

$$(\sigma_0, \sigma_1, \sigma_2) = (0, 0, 0) \tag{30}$$
$$= (1, 1, 1) \tag{31}$$
$$= (-1, -1, 1) \tag{32}$$
$$= (1, -1, -1) \tag{33}$$
$$= (-1, 1, -1) \tag{34}$$

The last four correspond to the minima for general rigid rotation, and 180° rotations about each coordinate axis in stretch space. The $(0, 0, 0)$ corresponds to the maximum induced by the origin barrier.

3.2 Locating Minima Under Uniform Scaling

We now analyze the uniform scaling case, and characterize the critical points that appear. Following from the previous section, this constitutes a complete characterization of all the critical points in the energy.

Under a uniform scaling δ, the energy becomes:

$$\Psi = \frac{\mu}{2}(3\delta^2 - 3) - \mu\left(\frac{3}{4}\delta^3 - 1\right) + \frac{\lambda}{2}(\delta^3 - 1)^2 - \frac{\mu}{2}\log\left(3\delta^2 + 1\right). \tag{35}$$

We can again divide through by μ to obtain $\beta = \frac{\lambda}{\mu}$ and solve for the critical points using Mathematica:

```
beta =.
Psi = (1/2) (3 x^2 - 3) - ((3/4) x^3 - 1) +
(beta/2) (x^3 - 1)^2 - (1/2) Log[3 x^2 + 1]
P = D[Psi, x]
solution = Solve[{P == 0}, x]
```

This solve finds a double root at $\delta = 0$, one at $\delta = 1$, and four additional roots that do not have simple expressions. The first two are always complex, so they require no further examination. The second two become real-valued at a sufficiently low threshold for β. When they becomes real-valued, they represent spurious critical points, so we should characterize the settings of β where the complex-to-real transition occurs. Fortunately, the two roots become real-valued at the same moment; their imaginary components are identical up to a sign change. Therefore, examining the transition point of one of them suffices.

Solving for the transition point symbolically can be difficult, because the imaginary component flattens out to zero at the critical moment, so phrasing the problem in terms of root-finding is ambgiuous because there are infinitely many solutions. Instead, we take a numerical approach in Matlab. The code that evaluates the relevant root is as follows:

```
function [result] = root(beta)
result = ...
(-1/4)+(1/2).*((-23/36)+(1/9).*2.^(-1/3).*beta.^(-1).*(189.* ...
beta+172.*beta.^2).*(6561.*beta+(-9396).*beta.^2+(-8320).* ...
  beta.^3+9.*3.^(1/2).*(177147.*beta.^2+(-951912).*beta.^3+( ...
  -1299600).*beta.^4+(-461056).*beta.^5+(-50176).*beta.^6).^( ...
  1/2)).^(-1/3)+(1/18).*2.^(-2/3).*beta.^(-1).*(6561.*beta+( ...
 -9396).*beta.^2+(-8320).*beta.^3+9.*3.^(1/2).*(177147.* ...
beta.^2+(-951912).*beta.^3+(-1299600).*beta.^4+(-461056).* ...
 beta.^5+(-50176).*beta.^6).^(1/2)).^(1/3)).^(1/2)+(1/2).*(( ...
 -23/18)+(-1/9).*2.^(-1/3).*beta.^(-1).*(189.*beta+172.* ...
beta.^2).*(6561.*beta+(-9396).*beta.^2+(-8320).*beta.^3+ ...
 9.*3.^(1/2).*(177147.*beta.^2+(-951912).*beta.^3+(-1299600).* ...
  beta.^4+(-461056).*beta.^5+(-50176).*beta.^6).^(1/2)).^( ...
 -1/3)+(-1/18).*2.^(-2/3).*beta.^(-1).*(6561.*beta+(-9396).* ...
 beta.^2+(-8320).*beta.^3+9.*3.^(1/2).*(177147.*beta.^2+( ...
-951912).*beta.^3+(-1299600).*beta.^4+(-461056).*beta.^5+( ...
 -50176).*beta.^6).^(1/2)).^(1/3)+(1/4).*((13/3)+(-2/3).* ...
beta.^(-1).*((-9)+4.*beta)).*((-23/36)+(1/9).*2.^(-1/3).* ...
beta.^(-1).*(189.*beta+172.*beta.^2).*(6561.*beta+(-9396) ...
  .*beta.^2+(-8320).*beta.^3+9.*3.^(1/2).*(177147.*beta.^2+( ...
  -951912).*beta.^3+(-1299600).*beta.^4+(-461056).*beta.^5+( ...
  -50176).*beta.^6).^(1/2)).^(-1/3)+(1/18).*2.^(-2/3).*beta.^( ...
  -1).*(6561.*beta+(-9396).*beta.^2+(-8320).*beta.^3+9.*3.^( ...
  1/2).*(177147.*beta.^2+(-951912).*beta.^3+(-1299600).* ...
beta.^4+(-461056).*beta.^5+(-50176).*beta.^6).^(1/2)).^(1/3) ...
  ).^(-1/2)).^(1/2);
```

We ran a midpoint search to double precision and located the transition point at $\beta = 0.152568262069702$. This is the smallest setting of β where the spurious root does not appear. This corresponds to $\nu \approx -0.85102$, which is more precise than the $\nu \in (-1, -\frac{1}{2})$ bound that was empirically observed in Figs. 5(a) and 5(c)

The exact shape of the energy at this moment can be seen in Fig. 5(b). This is the moment when the critical point first appears as an inflection point, but has not yet become a minimum. The stable settings for our material model can thus be stated more precisely as $\nu \in [-0.851, 0.5)$, though it is really only recommended for $\nu \in [0, 0.5)$. From a practical standpoint, this means that if we pin $\mu = 1$, then the stable region is $\lambda \in [0.1526, \infty)$.

REFERENCES

O. Civit-Flores and A. Susín. 2014. Robust Treatment of Degenerate Elements in Interactive Corotational FEM Simulations. *Comput. Graph. Forum* 33, 6 (2014), 298–309.

G. Irving, J. Teran, and R. Fedkiw. 2004. Invertible Finite Elements for Robust Simulation of Large Deformation. In *ACM SIGGRAPH/Eurographics Symp. Comp. Anim.* 131–140.

Ryo Kikuuwe, Hiroaki Tabuchi, and Motoji Yamamoto. 2009. An Edge-based Computationally Efficient Formulation of Saint Venant-Kirchhoff Tetrahedral Finite Elements. *ACM Trans. Graph.* 28, 1, Article 8 (2009), 13 pages.

Alexey Stomakhin, Russell Howes, Craig Schroeder, and Joseph M. Teran. 2012. Energetically Consistent Invertible Elasticity. In *ACM SIGGRAPH/Eurographics Symp. Comp. Anim.* 25–32.

Joseph Teran, Eftychios Sifakis, Geoffrey Irving, and Ronald Fedkiw. 2005. Robust Quasistatic Finite Elements and Flesh Simulation. In *ACM SIGGRAPH/Eurographics Symp. Comp. Anim.* 181–190.